IEEE Access
Multidisciplinary | Rapid Review | Open Access Journal

Received November 6, 2020, accepted November 22, 2020, date of publication December 30, 2020,
date of current version January 12, 2021.

Digital Object Identifier 10.1109/ACCESS.2020.3048181

Mixed Noise Removal Using Adaptive Median Based Non-Local Rank Minimization

DAI-GYOUNG KIM[1], MUKHTAR HUSSAIN[2], MUHAMMAD ADNAN[2], MUHAMMAD ASIF FAROOQ[3], ZAHID HUSSAIN SHAMSI[2], AND ASIF MUSHTAQ[4]

[1]Department of Applied Mathematics, Hanyang University (ERICA), Ansan 15588, South Korea
[2]Department of Mathematics, University of the Punjab, Lahore 54590, Pakistan
[3]School of Natural Sciences, NUST, Islamabad 44000, Pakistan
[4]Fakultet for lærerutd., kunst og kultur, Nord Universitet, 8049 Bodø, Norway

Corresponding author: Asif Mushtaq (asif.mushtaq@nord.no)

This work was supported by the Institute of Information and Communications Technology Planning and Evaluation (IITP) Grant funded by the Korean Government (MSIT), Artificial Intelligence Convergence Research Center, Hanyang University (ERICA), under Grant 2020-0-01343.

ABSTRACT In this paper, we present an innovative mechanism for image restoration problems in which the image is corrupted by a mixture of additive white Gaussian noise (AWGN) and impulse noise (IN). Mixed noise removal is much more challenging problem in contrast to the problems where either only one type of noise model (either Gaussian or impulse) is involved. Several well-known and efficient algorithms exist to effectively remove either Gaussian noise or Impulse noise, independently. However, in practice, noise may occur as a mixture of such noise models. Thus, the existing techniques devised to handle individual types of noise may not perform well. Moreover, the complexity of the problem hinges on the fact that the removal of either type of noise from the given image affects the noise statistics in the residual image. Therefore, a rigorous mechanism is required which not only infers altered noise statistics but also removes the residual noise in an effective manner. In this regard, an innovative approach is introduced to restore the underlying image in three key steps. Firstly, the intensity values, affected by impulsive noise, are identified by analyzing noise statistics with the help of adaptive median filtering. The identified intensity values are then aggregated by exploiting nonlocal data redundancy prior. Thus the first step enables the remaining noise to follow the zero mean Gaussian distribution in the median filtered image. Secondly, we estimate Gaussian noise in the resulting image, which acts as a key parameter in the subsequent singular value thresholding process for rank minimization. Finally, a reduced rank optimization applied to the pre-processed image obtained in the first step. The experimental results indicate that the proposed AMNLRA (Adaptive Median based Non-local Low Rank Approximation) approach can effectively tackle mixed noise complexity as compared to numerous state of the art algorithms.

INDEX TERMS Image denoising, low rank approximation, mixed noise, nuclear norm, rank minimization, similarity measure, singular value decomposition.

I. INTRODUCTION

Image restoration is a well known inverse problem with the aim of extracting the underlying true image from the observed noisy image. Although image restoration, specifically, image denoising is an extensively studied problem yet it remains a challenging task since image denoising is an ill-posed inverse problem in mathematical perspective and does not admit a unique optimal solution. In addition, the problem becomes more complicated in case of the noise model which is a mixture of two different noise distributions. Mixed noise, for instance, can be a combination of additive white Gaussian noise (AWGN) and impulse noise (IN) caused due to multiple noise sources during image acquisition process

Additive White Gaussian Noise is the most widely used model of noise, characterized by adding zero-mean Gaussian distribution to each intensity value of an image. Different techniques have been proposed in order to remove AWGN. Conventional linear filters, including mean filtering, effectively remove the noise but simultaneously distort the important features of the image like edges and textures. In order to address this problem nonlinear filtering techniques have

The associate editor coordinating the review of this manuscript and approving it for publication was Hengyong Yu.

been proposed. Tomasi and Maduchi [1] proposed Bilateral Filtering (BF) by estimating each pixel using the weighted average of neighbouring pixels, and considered both spatial and intensity information to calculate the weight. Buades *et al.* [2] extended the idea of BF and proposed Non-Local mean (NLM) algorithm by taking weighted average of patches instead of pixels. To further enhance NLM based denoising approach, several techniques were proposed. Dabov *et al.* [3], for instance, suggested BM3D by collecting the related patches in a 3-D tensorial form and used spectral transforms to shrink these tensors for noise removal. Recently, sparse representation and dictionary learning based algorithms gained substantial interest. Centralized sparse representation (CSR) [4] provided promising results by joint application of non local information and sparse representation. Dong *et al.* [5] generalized Bayesian based shrinkage by connecting the low-rank approximation with simultaneous sparse coding (SAIST) in an iterative fashion. Gu *et al.* [6] proposed weighted nuclear minimization (WNNM) by shrinking the singular values of similar patch matrices while considering corresponding weights.

Impulse noise (IN), in contrast to Gaussian noise, is characterized by replacing a portion of pixels with random noise value, and the rest of the pixels remain unchanged. There are two types of IN, namely, salt-and-pepper impulse noise (SPIN) and random valued impulse noise (RVIN). Owing to good denoising property and high computational performance, nonlinear filters such as the median filter and its modified versions were mainly used to remove IN noise [7]–[10].

It is relatively less challenging to address either AWGN or IN where noise statistics follow a single noise distribution. However, in many practical situations, image is degraded by a mixture of different types of noise like SPIN+AWGN or RVIN+AWGN. In such scenario, restoration of underlying image data becomes more involved. In order to remove mixed noise, several techniques have been proposed where both noise statistics are dealt simultaneously [11], [12]. Despite pioneering contributions of these techniques, their performance is limited as simultaneous treatment of mixed noise distributions of different kinds ceases to capture noise complexity effectively. Later on, more effective techniques based on the combination of variational and non-local mechanism are proposed [13]–[16]. The majority of the recent methods relies on detection based approaches [17]–[20] where the pixels with impulse noise traces are first detected. Garnett *et al.* [18], for instance, suggested a trilateral filtering mechanism which involves detection of IN by considering rank-order statistics and gradient information. Furthermore, some of these techniques also exploited low rank approximation in this regard [17], [20]. In addition, sparsity based dictionary learning approaches have also been suggested to address mixed noise removal problems. These approaches combine certain variants of median filtering [10], [21] with subsequent dictionary learning process [22]–[25].

As discussed above, the existing two phase methods require two sequential steps for mixed noise removal. That is, detection of IN affected pixels followed by AWGN removal. Such two phase techniques are effective in cases where mixing ratio of impulse noise is small and added Gaussian noise has small noise variance. However, in case of higher mixing ratio of impulse noise and large variance of Gaussian noise, these techniques yield limited performance as comprehensively discussed later in the experimental section. This limited performance of existing approaches is based on the argument that the residual noise in the image obtained after median-type filtering follows Gaussian distribution which is not the case. In fact, the distribution of the residual noise is far from Gaussian distribution. However, owing to certain suitable operations, on filtered images obtained in the first phase, the residual noise distribution may be transformed to follow Gaussian distribution. After transforming residual noise to follow Gaussian distribution, the next challenging task is to infer the noise distribution of the Gaussian mixture, namely, the additive Gaussian noise originally added to the image and the Gaussian distribution obtained by processing median-filtered image. Once the Gaussian mixture is obtained and estimated, the problems become less complicated and can be addressed by exploiting well-known image priors like sparsity, non-locality and reduced rank property.

With these key motivations, we propose an innovative algorithm Adaptive Median Nonlocal Low Rank Approximation (AMNLRA) which consists of three steps: In the first step, the noise statistics are examined to identify the pixel locations susceptible to impulse noise. These identified pixels are further processed using nonlocal means filtering (NLM) by exploiting data redundancy prior. NLM processing transforms the residual noise into Gaussian noise distribution. In the second step, the Gaussian noise is estimated in the preprocessed image which plays a pivotal role in the subsequent thresholding process. Finally, a rank minimization strategy is utilized to obtain the final denoised image. Experimental results show that the suggested mechanism can capture and handle the complexity of mixed noise effectively as compared to various most advanced denoising algorithms.

The rest of this paper is organized as follows: In Section. II, we present various noise models for mixed noise and briefly discuss existing techniques pertinent to individual noise components of mixed noise distribution. The proposed algorithm is presented in Section. III. Section. IV entails the experimental results and comparison with the benchmark existing algorithms. Finally, in Section. V conclusions are drawn regarding the efficacy of the proposed algorithm.

II. PRELIMINARIES

A. NOISE MODEL

Let U be an observed noisy image and $u(i, j)$ be the intensity at location (i, j). Suppose that V represents the underlying noise free image. In case of AWGN, the noise model can be defined as

$$U = V + N, \tag{1}$$

where N represents the additive zero-mean white Gaussian noise. Impulse noise (IN) which is second ingredient of mixed noise model, has two well known variants namely, salt and pepper impulse noise (SPIN) and random value impulse noise (RVIN). Let the dynamic range of the noisy image U be denoted as $[d_{min}, d_{max}]$, then AWGN+SPIN mixed noise model can be described as:

$$U_{i,j} = \begin{cases} d_{min}, & \text{with the probability } \frac{S}{2}; \\ d_{max}, & \text{with the probability } \frac{S}{2}; \\ V_{i,j} + N_{i,j}, & \text{with probability } 1 - S\ . \end{cases} \tag{2}$$

Similarly, in case of RVIN the pixel may assume any intensity value in between the dynamic range with certain probability. The AWGN+RVIN noise model can be described as:

$$U_{i,j} = \begin{cases} d_{i,j}, & \text{with probability } S; \\ V_{i,j} + N_{i,j}, & \text{with probability } 1 - S\ . \end{cases} \tag{3}$$

B. MEDIAN FILTER AND ADAPTIVE MEDIAN FILTER

The median filter is a statistical non-linear signal processing technique suggested by Tukey [26] to remove noise from a noisy image. In this method, the noisy value of the image is replaced by the median of the neighbourhood (window). The mask's pixels are grouped according to their respective grey intensity value and the group's median is stored to replace the noisy value. Mathematically, this simple filtering process can be written as:

$$g(i,j) = med\{f(i-x, j-y), (x,y) \in W\}, \tag{4}$$

where $f(i,j)$ and $g(i,j)$ are the input noisy image and median filtered image, respectively. W is the two dimensional window of size $m \times m$ (m is commonly odd) with center at location (i,j). The median filter works well, but fails when the probability of the impulse noise occurrence is high. In order to address this issue, several variants of median filtering [21], [27]–[31] have been proposed. Among these variants, adaptive median filter [21] gained much attention owing to its mask size adaptivity corresponding to noisy data. In this approach, an adaptive window of odd size $2n+1$, where n varies from 1 to N, is used to process the center pixel. The neighboring pixels in the window are assorted according to their intensity values. Further, these values are used to determine whether the central pixel location is affected by impulse noise or not. In case, the central pixel is affected by impulse noise, it is replaced by the median of assorted neighborhood pixel values. An alternative adaptive median filtering is the center weighted median (CWM) filtering technique [10]. The key concept in this approach is to assign a weight to the central pixel of the confining window or mask. The output,$m(i,j)$ of CWM having window of size w and center weight $2k+1$ can be represented by [10]

$$m(i,j) = med\{u(((w+1)/2) - k; w), u(i,j), u(((w+1)/2) + k; w)\}, \tag{5}$$

where $u(n; w)$ indicates the n^{th} smallest sample among the w samples within the window and $u(i,j)$ is the input noisy pixel value at the center of the window.

C. LOW RANK APPROXIMATION

Rank minimization mechanism, generally known as low rank approximation, is one of the most effective approaches for Gaussian noise removal [4], [6], [32]–[34] in recent years. More recently, in addition to Gaussian noise model, low rank approximation has been successfully applied to a variety of noise models such as speckle noise and seismic noise models [35]–[37]. Essence of low rank approximation for image denoising lies in construction of a matrix M using similar patches from the given noisy image. That is, each column of M is a vectorized version of a patch, say $\mathbf{p}_i$, similar to the reference image patch, $\mathbf{p}$, under consideration. Similarity of these stacked patches leads to essentially a low rank matrix [4]. Prior to application of low rank techniques to image denoising, it has been successfully employed to data intensive matrix completion problem where the matrix is to be recovered using only a few of its available entries [4], [38]–[43]. In fact, rank minimization or low rank approximation is known to be a non-convex problem and therefore it lacks the assurance of global optimal solution through conventional convex optimization techniques. However, proximal optimal solution can be obtained by replacing rank minimization constraint with nuclear norm minimization (NNM) which is a convex regularization of original non-convex problem. Reference [22] NNM based algorithms aim to find the best possible approximation R of given data S subject to the constraint that R should have reduced rank. Mathematically, NNM can be described as:

$$\hat{R} = \underset{R}{argmin} \|R - S\|_F^2 + \lambda \|R\|_*, \tag{6}$$

where $\|.\|$ represents the Frobenius norm, $\|.\|_* = \sum_i |\pi_n(R)|$ is the nuclear norm, π_n is n^{th} singular value of R and λ is the regularization parameter. The closed-form solution of Eq. 6 is given as [22]:

$$\hat{R} = PD_\lambda(\Sigma)Q^T, \tag{7}$$

where $S = P\Sigma Q^T$ denotes the SVD of S and $D_\lambda(\Sigma) = max(\Sigma - \lambda I, 0)$ is SVD thresholding parameter. Although NNM based optimization serves as convex regularization of rank minimization, it has limited performance in image restoration applications due to the following two major reasons. Firstly, note that in Eq. 6, NNM assigned equal weights to each singular value. Secondly, it can be observed that regardless of magnitudes of singular values, each singular value is shrunk with same penalty λ. However, larger singular values do have more importance than the smaller ones in physical settings and therefore such large singular values should be shrunk with less penalty. As a result of these limitations, the denoising capabilities of NNM are not so

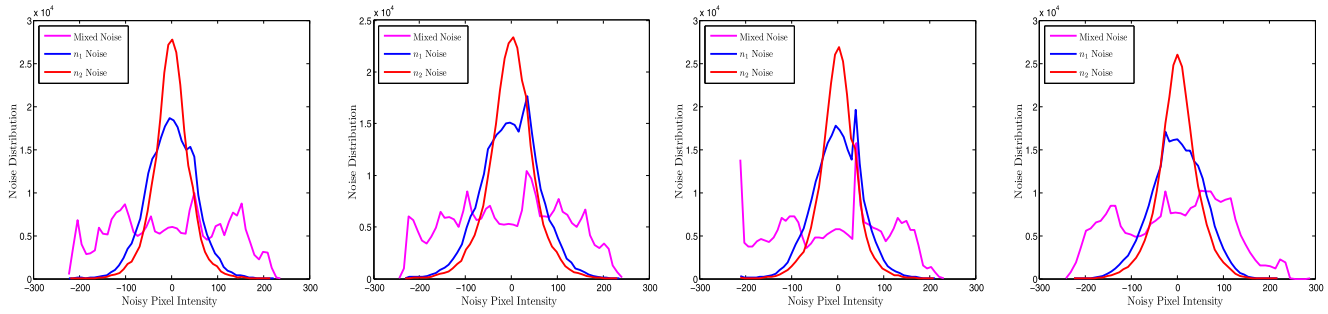

FIGURE 1. Visualization of Noise Distributions: Mixed Noise initially added is represented by magenta color. Noise distribution n_1 after adaptive median filtering step is depicted by blue color and Noise distribution n_2 after Non-local Means filtering step is represented by red color. Test images used in the plots are (a) Lena, (b) Barbara, (c) Man and (d) Hill, respectively.

promising. In order to have proportionate shrinking of singular values, weighted NNM (WNNM) was suggested as follows [6],

$$\hat{R} = \underset{R}{\operatorname{argmin}} \|R - S\|_F^2 + \lambda \|R\|_{w,*}, \tag{8}$$

where $\|R\|_{w,*} = \sum_i | w_i \pi_n(R)|$ is the weighted nuclear norm. Despite being non-convex optimization problem, WNNM may converge to an optimal solution provided that the weights w_i are in ascending order. The interested readers are referred to [6] for details of convergence analysis. The closed form solution of Eq. 8 is:

$$\hat{R} = PD_{w_i}(\Sigma)Q^T, \tag{9}$$

where $D_{w_i}(\Sigma) = max(\Sigma - w_i, 0)$.

III. PROPOSED ALGORITHM

In this section, we present our proposed mechanism which consists of three key steps namely, identification and replacement of pixels affected by impulse noise followed by noise estimation strategy to determine the noise characteristics in the image obtained in first step. Lastly, based on noise estimation, suitable rank minimization approach is utilized to recover the final denoised image.

A. PREPROCESSED IMAGE

Suppose that the observed image u with size $R^{M\times N}$ and indexing set $\Omega = i, i = 1, 2, \ldots, MN$ is affected by mixed noise, i.e., impulse noise (IN) and additive white Gaussian noise (AWGN). As a first major step, we analyse the noise statistics to locate and identify the pixel values affected by IN. For this purpose, we employ adaptive median filter (AMF) [21]. By examining each pixel similarity with its neighbouring pixels (within a window of certain size), AMF classifies pixels as affected or not affected by impulse noise. The size of the neighbourhood window and the threshold for the comparison are adjustable. A pixel that is different from a majority of its neighbour is marked as impulse noise. Such pixels are replaced by the median of neighboring pixels in the local neighborhood window. As a result, we obtain the following filtered image y,

$$y = AMF(u). \tag{10}$$

Based on above identification and replacement process, the pixels in y can now be classified into two disjoint categories. The collection Δ, of pixels corrupted by IN defined as:

$$\Delta = \{i \in \Omega | y(i) - u(i) \neq 0\}. \tag{11}$$

Rest of the pixels, affected by AWGN, are grouped into the collection, R, defined as

$$R = \Omega \setminus \Delta, \tag{12}$$

Before, proceeding further, let us first analyze the noise statistics in the filtered image y. That is, we want to determine whether the noise in y follows Gaussian distribution or not. For this purpose, let the noise in y be denoted by $n_1 = y - V$, where V represents the original noise free image which is assumed to be available for the sake of analysis. It turned out that n_1 noise does not follow Gaussian distribution as shown in Fig. 1. Based on this analysis, a question naturally arises regarding the source of non Gaussianity in n_1 noise distribution. Obviously, by its construction, R, can not be identified as possible source. Thus, only possible source for non-Gaussianity lies in the set Δ.

Despite the existence of several effective approaches for impulse noise filtering, the noise cannot be removed completely. To worsen the situation, the remnant impulse noise may affect the Gaussian noise distribution adversely. Therefore, in order to mitigate the effects of remnant impulse noise on Gaussian noise, we exploit non-local means filtering [2] as follows. Note that the noise distribution n_1 is not Gaussian, yet it can be transformed to a Gaussian distribution using non-local self similarity (NSS) prior [2], [44] to the pixel values affected by impulse noise (pixel location stored in the set Δ). That is, for a given image patch (rather than individual pixel) within an image can be approximated by finding and then aggregating the similar patches in that image. As shown in Eqs. (11-12), the pixels in y can be divided into two categories R and Δ. Since Δ set is responsible for non-Gaussianity of n_1, therefore it seems justifiable to apply

non-local means filtering [2] to pixels located in Δ, whereas the pixels in set R should remain unchanged. The NLM, u_n^i, of pixel $y(i)$ with patch $\mathcal{P}(y_i)$ (patch centered at location i) in the set Δ is defined as [2]:

$$u_n^i = \frac{1}{K} \sum_{j \in w_i;\ j \in \Delta} C(i,j)\mathcal{P}(y_j), \tag{13}$$

where $C(i,j) = e^{-\frac{\|\mathcal{P}(y_i)-\mathcal{P}(y_j)\|^2}{h^2}}$ is the similarity weight of patch centered at $y(j)$ with the reference patch centered at $y(i)$ and w_i is the search window centered at pixel location $i \in \Delta$. The denominator, K defined by

$$K = \sum_{i \in \Delta} \sum_{j \in w_i;\ j \in \Delta} C(i,j), \tag{14}$$

refers to the normalization constant. Let u_n be the resultant image obtained by applying NLM on y. It can be observed from Fig. 1 that residual noise, n_2, in the image u_n, follows Gaussian distribution, with zero mean, to a great extent. Further, using disjoint sets Δ and R, we can construct an indicator matrix β (with entries either 0 or 1) as follows:

$$\beta = \begin{cases} 0, & \text{if } i \in \Delta; \\ 1, & \text{Otherwise.} \end{cases} \tag{15}$$

Finally, we are in a position to define our first phase (preprocessed) image, u_p, in which noise distributions are Gaussian with zero means. The preprocessed image is mathematically expressed as:

$$u_p = \beta u + (\mathbb{I} - \beta)u_n, \tag{16}$$

where $\mathbb{I}$ is a matrix with all entries 1. Further, it can be observed that Gaussian noise distributions in u_p are independent since the image components βu and $(\mathbb{I}-\beta)u_n$ are disjoint by virtue of indicator matrix β.

B. NOISE ESTIMATION

It is worth noticing that u_p in Eq. (16) is a convex combination of two noise images namely, the given noisy image u with Gaussian noise having known standard deviation σ and the preprocessed noisy image u_n with Gaussian noise n_2 but with standard deviation which is yet unknown. Thus, prior to any further denoising operations on u_p, it is of utmost importance to find standard deviation of n_2 noise distribution. To estimate noise level of a noisy image various block base and wavelet based techniques have been suggested [45]–[48]. Basic principle of these filter based techniques is that low pass filter is applied to the noisy image first and the variance is subsequently estimated from the difference between the observed noisy image and the filtered image. Alternatively, patch based strategies have been envisaged for noise estimation in recent years [49]–[53]. Among these approaches, we follow the principal component analysis (PCA) based mechanism adopted in [53].

That is, we estimate standard deviation of noise n_2 using the minimal eigenvalue of the covariance matrix Υ which is defined as:

$$\Upsilon = \frac{1}{k} \sum_{i=1}^{k} (p_i - \upsilon)(p_i - \upsilon), \tag{17}$$

where $\upsilon = \frac{1}{k}\sum(p_i)$ and k represents the mean and the number of compared patches, respectively. The standard deviation, σ_n, of noise distribution, n_2, in the image u_n can then be calculated as:

$$\sigma_n = \min_{1 \le i \le k} \lambda_i, \tag{18}$$

where λ_i is the eigenvalue of the low rank covariance matrix, υ. Finally, the preprocessed image u_p defined by Eq. (16) contains the noise which is a mixture of two independent Gaussian distributions with standard deviations σ and σ_n, respectively, and having zero means. The independence of these distribution is guaranteed due to indicator matrix β defined in Eq. (15). Thus, the mixture noise in u_p, being sum of two independent normal distributions is simply another normal distribution with mean $\mu_p = 0$ and variance σ_p^2 defined by

$$\sigma_p^2 = \sigma^2 + \sigma_n^2. \tag{19}$$

C. RANK MINIMIZATION STRATEGY

As discussed above, the preprocessed image is now affected by Gaussian noise only. In order to remove Gaussian noise, several effective approaches have been suggested as described briefly in Section. I. However, owing to the superior performance and simplicity, low rank based approaches are prevalent [4], [6], [34] as discussed in Section. II. Here, we employ the rank minimization process adopted in [6], [34] as follows. The preprocessed noisy image, u_p can be modeled as:

$$u_p = v + \mathcal{N}\left(0, \sigma_p^2\right), \tag{20}$$

where v is the desired underlying image to be recovered and $\mathcal{N}\left(0, \sigma_p^2\right)$ is Gaussian noise distribution given by Eq. (19). Afterwards, patch based comparison is performed on the given image u_p to constitute patch matrices for each pixel location in u_p. Mathematically this construction of patch matrices can be modelled as [6], [34]:

$$\mathbf{U}_{p_i} = \mathbf{V}_i + \mathcal{N}_i, \tag{21}$$

where $\mathbf{U}_{p_i}$ is the patch matrix formed by stacking the noisy patches similar to the reference patch p_i centered at pixel location i in image u_p. $\mathbf{V}_i$ and $\mathcal{N}_i$ are corresponding patch matrices at pixel location i in v and $\mathcal{N}\left(0, \sigma_p^2\right)$. It can be noticed that the patch matrix $\mathbf{U}_{p_i}$ is inherently a low rank matrix as it consists of similar image patches.

Our main goal is to search for best approximation, $\hat{\mathbf{V}}_i$, for the underlying noise free patch matrix $\mathbf{V}_i$. To serve the purpose, we solve the following rank minimization problem [6]:

$$\hat{\mathbf{V}}_i = argmin \frac{1}{2\sigma_p^2} \|\mathbf{U}_{p_i} - \mathbf{V}_i\|_F^2 + \eta \|\mathbf{V}_i\|_{w,*}, \tag{22}$$

TABLE 1. PSNR(dB) and FSIM comparison of the proposed algorithm (AMNLRA) with other methods for mixed noise (AWGN+SPIN).

	$S=30\%$					$S=40\%$				$S=50\%$			
Image	σ	Cai et al.	l_1-l_0	WESNR	AMNLRA	Cai et al.	l_1-l_0	WESNR	AMNLRA	Cai et al.	l_1-l_0	WESNR	AMNLRA
Lena	10	31.76	**33.52**	33.22	33.07	31.01	32.59	**32.72**	31.92	30.14	31.60	**31.93**	31.00
		0.9629	**0.9717**	0.9704	0.9702	0.9560	0.9665	**0.9670**	0.9600	0.9458	0.9594	**0.9618**	0.9600
	20	29.34	30.76	30.73	**31.01**	28.96	30.01	30.27	**30.44**	28.42	29.27	29.68	**29.77**
		0.9315	0.9430	0.9419	**0.9500**	0.9263	0.9395	0.9375	**0.9402**	0.9181	0.9288	0.9301	**0.9303**
	25	28.33	29.78	29.85	**30.13**	28.04	29.25	29.42	**29.69**	27.56	28.45	28.79	**29.00**
		0.9315	0.9430	0.9419	**0.9500**	0.9263	0.9395	0.9375	**0.9402**	0.9018	0.9288	0.9301	**0.9303**
Couple	10	28.53	**31.12**	30.55	29.84	27.66	**29.92**	29.84	28.86	26.73	28.81	**28.95**	28.00
		0.9437	**0.9671**	0.9626	0.9601	0.9284	**0.9577**	0.9561	0.9500	0.9063	0.9438	**0.9460**	0.9400
	20	26.81	28.36	28.08	**28.08**	26.25	27.51	27.55	**27.58**	25.57	26.64	26.85	**26.86**
		0.9128	0.9314	0.9252	**0.9300**	0.8973	0.9142	0.9156	**0.9200**	0.8753	0.9012	0.9023	**0.9100**
	25	26.07	27.12	27.18	**27.30**	25.60	26.50	26.68	**26.76**	25.02	25.89	26.03	**26.08**
		0.8976	0.9042	0.9053	**0.9120**	0.8827	0.8924	0.8949	**0.9010**	0.8615	0.8824	0.8841	**0.8906**
Fingerprint	10	27.44	**29.26**	28.91	28.66	26.13	27.75	**28.07**	27.40	24.43	26.12	**27.04**	26.30
		0.9771	**0.9836**	0.9830	0.9810	0.9652	0.9747	**0.9781**	0.9720	0.9418	0.9601	**0.9706**	0.9620
	20	24.66	26.09	26.17	**26.54**	23.82	25.23	25.63	**25.80**	22.60	24.08	24.93	**24.95**
		0.9542	0.9641	0.9647	**0.9700**	0.9381	0.9542	0.9580	**0.9600**	0.9083	0.9387	0.9499	**0.9500**
	25	23.67	25.16	25.21	**25.66**	22.92	24.35	24.72	**25.07**	21.85	23.25	24.08	**24.19**
		0.9424	0.9532	0.9537	**0.9600**	0.9246	0.9434	0.9474	**0.9503**	0.8930	0.9258	0.9396	**0.9489**
Hill	10	29.78	**31.72**	31.01	30.75	29.14	**30.85**	30.51	30.01	28.42	**29.99**	29.87	29.19
		0.9474	**0.9656**	0.9595	0.9570	0.9358	**0.9574**	0.9539	0.9500	0.9193	**0.9463**	0.9457	0.9430
	20	27.89	28.81	28.71	**28.83**	27.50	28.27	28.33	**28.35**	26.98	27.69	27.77	**27.79**
		0.9101	0.9246	0.9226	**0.9300**	0.8972	0.9133	0.9138	**0.9200**	0.8792	0.9013	0.9030	**0.9100**
	25	27.08	27.91	27.93	**28.03**	26.73	27.48	27.55	**27.71**	26.23	26.93	27.06	**27.15**
		0.8904	0.9039	0.9044	**0.9101**	0.8779	0.8950	0.8960	**0.9000**	0.8601	0.8819	0.8834	**0.8896**
Man	10	29.73	**31.45**	30.81	30.59	29.01	**30.49**	30.22	29.62	28.19	29.43	**29.48**	28.61
		0.9497	**0.9647**	0.9605	0.9601	0.9379	**0.9559**	0.9546	0.9530	0.9213	0.9435	**0.9461**	0.9420
	20	27.83	28.45	28.48	**28.58**	27.38	27.93	28.03	**28.10**	26.82	27.32	27.48	**27.52**
		0.9161	0.9225	0.9233	**0.9281**	0.9041	0.9126	0.9136	**0.9223**	0.8876	0.9027	0.9035	**0.9101**
	25	26.99	27.59	27.65	**27.82**	26.60	27.05	27.23	**27.40**	26.09	26.45	26.72	**26.77**
		0.8973	0.9057	0.9066	**0.9149**	0.8854	0.8955	0.8962	**0.9040**	0.8682	0.8842	0.8857	**0.8912**
Boat	10	28.79	**31.43**	30.60	30.40	27.91	**30.33**	29.86	29.70	26.90	**29.03**	28.92	28.80
		0.9462	**0.9685**	0.9618	0.9599	0.9326	**0.9594**	0.9554	0.9523	0.9104	**0.9463**	0.9457	0.9381
	20	27.09	**28.71**	28.19	28.27	26.50	**27.74**	27.61	27.64	25.77	26.76	26.85	**26.90**
		0.9128	**0.9321**	0.9250	0.9307	0.8988	**0.9171**	0.9157	0.9135	0.8785	0.9028	0.9038	**0.9090**
	25	26.32	27.29	27.30	**27.50**	25.84	26.68	26.74	**26.86**	25.16	25.96	26.03	**26.14**
		0.8956	0.9074	0.9085	**0.9152**	0.8829	0.9003	0.9011	**0.9050**	0.8623	0.8857	0.8866	**0.8956**
Average	10	29.34	**31.46**	30.85	30.55	28.47	**30.32**	30.20	29.58	27.46	29.16	**29.36**	28.65
		0.9545	**0.9711**	0.9663	0.9647	0.9426	**0.9619**	0.9608	0.9562	0.9241	0.9492	**0.9526**	0.9475
	20	27.27	28.53	28.39	**28.55**	26.73	27.78	27.90	**27.98**	21.76	26.96	27.26	**27.30**
		0.9229	0.9363	0.9337	**0.9398**	0.9103	0.9251	0.9257	**0.9293**	0.8911	0.9125	0.9154	**0.9199**
	25	26.41	27.47	27.52	**27.74**	25.95	26.88	27.05	**27.25**	25.31	26.15	26.45	**26.56**
		0.9091	0.9195	0.9200	**0.9270**	0.8966	0.9110	0.9121	**0.9167**	0.8771	0.8981	0.9015	**0.9077**

where $\|\cdot\|_F$ and $\|\cdot\|_{w,*}$ are Frobenius and weighted nuclear matrix norms, respectively.

The above optimization problem can be solved by the following singular value decomposition:

$$(\mathbf{X}, \mathbf{D}, \mathbf{Y}) = svd(\mathbf{U}_{p_i}), \tag{23}$$

$$\hat{\mathbf{D}} = T_{w_i}(\mathbf{D}), \tag{24}$$

where T_{w_i} is the soft thresholding (shrinking) operator defined by

$$T_{w_i}(\mathbf{d}_{ii}) = sgn(\mathbf{d}_{ii})max(|\mathbf{d}_{ii}| - w_i, 0), \tag{25}$$

with $\mathbf{d}_{ii}$ being i^{th} diagonal element of $\mathbf{D}$. The thresholding weights, w_i, are defined as:

$$w_i = \frac{b\sqrt{m}}{d_{ii} + \kappa}, \tag{26}$$

where the constant $b > 0$ and m is the number of similar patches. To prevent possible division by zero, κ set as 10^{-6}. Finally, the approximation, $\hat{\mathbf{V}}_i$, for $\mathbf{V}_i$ is obtained as:

$$\hat{\mathbf{V}}_i = \mathbf{X}\hat{\mathbf{D}}\mathbf{Y}. \tag{27}$$

The above described minimization problem is solved for patch at location i in the image. This process is repeated for all the noisy patches extracted from the given noisy image u_p.

As a final step, the whole denoised image v can be obtained by aggregation of overlapping patches for each pixel location i in the image u_p. For sake of precise and succinct depiction, our proposed mechanism is summarized in Algorithm. 1.

IV. EXPERIMENTAL RESULTS

In order to conduct quantitative and qualitative comparison, the proposed algorithm (AMNLRA) is applied to ten frequently used gray scale test image with various textures which are shown in Fig. 2. Experiments were conducted to evaluate the performance of AMNLRA in comparison with the state-of-the-art mixed noise removal techniques, namely: Cai *et al.* [22], $l_1 - l_0$ [23], WESNR [17] and SNTP [54].

A. PARAMETER SETTING

The key feature of our proposed algorithm is the independent implementation of individual mechanisms, but connected through mediating step of effective noise estimation strategy. Therefore, in order to have fair comparison and

FIGURE 2. Benchmark test images used for quantitative and qualitative comparison.

TABLE 2. PSNR and FSIM comparison of the proposed algorithm (AMNLRA) with other methods for mixed noise (AWGN+SPIN), at $S = 50\%$.

	$\sigma = 20$			$\sigma = 30$			$\sigma = 50$			$\sigma = 70$		
Image	Cai et al.	WESNR	AMNLRA	Cai et al.	WESNR	AMNLRA	Cai et al.	WESNR	AMNLRA	Cai et al.	WESNR	AMNLRA
Lena	28.43	29.73	**30.00**	26.99	27.57	**28.47**	24.23	15.73	**26.58**	21.63	6.67	**25.21**
	0.9177	0.9300	**0.9348**	0.8905	0.9060	**0.9110**	0.8346	0.6222	**0.8703**	0.7867	0.5200	**0.8510**
Couple	24.44	26.71	**26.71**	24.31	25.10	**25.52**	22.31	14.52	**23.84**	20.57	6.63	**22.58**
	0.8664	0.9110	**0.9145**	0.8317	0.8801	**0.8890**	0.7669	0.6519	**0.8200**	0.7100	0.5007	**0.7642**
Boat	25.83	**26.95**	26.68	24.67	24.93	**25.74**	22.46	14.12	**24.14**	20.46	6.07	**23.00**
	0.8792	**0.9100**	0.9089	0.8470	0.8800	**0.8910**	0.7851	0.6277	**0.8200**	0.7258	0.5199	**0.7849**
Hill	27.11	27.77	**27.79**	25.94	26.38	**26.62**	24.57	15.99	**25.00**	21.18	7.94	**23.95**
	0.8886	0.9030	**0.9100**	0.8605	0.8809	**0.8925**	0.8072	0.6918	**0.8165**	0.7589	0.5078	**0.7745**
Man	26.90	27.48	**27.52**	25.70	25.94	**26.26**	23.30	15.27	**24.55**	20.86	7.23	**23.57**
	0.8909	0.9035	**0.9101**	0.8619	0.8830	**0.8883**	0.8070	0.6601	**0.8197**	0.7520	0.5269	**0.7944**
Fingerprint	22.56	24.93	**24.95**	20.91	23.25	**23.58**	18.32	10.26	**21.80**	16.66	5.18	**20.33**
	0.8999	0.9499	**0.9500**	0.8431	0.9309	**0.9324**	0.6910	0.7282	**0.8964**	0.5355	0.2956	**0.8465**
Average	25.87	27.26	**27.28**	24.75	25.52	**26.03**	22.53	14.31	**24.32**	20.22	6.62	**23.10**
	0.8904	0.9179	**0.9213**	0.8558	0.8934	**0.9007**	0.7819	0.6636	**0.8404**	0.7114	0.4784	**0.8025**

TABLE 3. PSNR and FSIM comparison of the proposed algorithm (AMNLRA) with other methods for mixed noise (AWGN+RVIN), at $\sigma = 10$.

	$r = 5\%$					$r = 10\%$					$r = 15\%$				
Image	Cai et al.	$l_1 - l_o$	WESNR	SNTP	AMNLRA	Cai et al.	$l_1 - l_o$	WESNR	SNTP	AMNLRA	Cai et al.	$l_1 - l_o$	WESNR	SNTP	AMNLRA
Lena	32.05	32.99	33.78	33.88	**34.12**	31.76	32.63	33.46	33.54	**33.78**	31.43	32.28	33.15	33.19	**33.33**
	0.9661	0.9650	0.9742	0.9748	**0.9770**	0.9643	0.9631	0.9729	0.9734	**0.9740**	0.9622	0.9611	0.9717	0.9720	**0.9735**
Boat	28.84	29.29	30.21	30.23	**30.45**	28.51	28.91	29.80	29.90	**30.13**	28.20	28.61	29.52	29.55	**29.61**
	0.9530	0.9508	0.9648	0.9650	**0.9680**	0.9494	0.9471	0.9619	0.9626	**0.9633**	0.9456	0.9439	0.9598	0.9600	**0.9610**
Couple	28.63	29.13	30.16	30.26	**30.30**	28.29	28.81	29.84	29.93	**29.96**	27.97	28.47	29.48	29.52	**29.54**
	0.9502	0.9477	0.9642	0.9646	**0.9660**	0.9467	0.9440	0.9619	0.9622	**0.9626**	0.9422	0.9399	0.9580	0.9584	**0.9595**
Fingerprint	28.47	29.73	30.15	30.39	**30.81**	27.97	29.12	29.63	29.76	**30.17**	27.44	28.47	29.03	29.10	**29.15**
	0.9852	0.9870	0.9885	0.9896	**0.9899**	0.9828	0.9844	0.9868	0.9879	**0.9883**	0.9797	0.9813	0.9847	0.9857	**0.9865**
Hill	29.94	30.17	30.96	30.98	**31.01**	29.72	29.95	30.69	30.75	**30.82**	29.48	29.70	30.46	30.50	**30.57**
	0.9540	0.9480	0.9634	0.9639	**0.9653**	0.9513	0.9554	0.9612	0.9618	**0.9630**	0.9481	0.9427	0.9591	0.9592	**0.9600**
Man	29.96	30.13	30.96	31.06	**31.15**	29.66	29.86	30.68	30.75	**30.84**	29.38	29.53	30.34	30.46	**30.49**
	0.9566	0.9500	0.9652	0.9655	**0.9666**	0.9537	0.9472	0.9628	0.9631	**0.9639**	0.9502	0.9437	0.9604	0.9607	**0.9620**
Peppers	31.65	32.23	32.80	**32.83**	32.40	31.00	31.73	32.24	32.11	**32.14**	30.52	31.16	31.77	31.68	**31.70**
	0.9688	0.9702	0.9758	**0.9761**	0.9736	0.9671	0.9685	0.9746	0.9739	**0.9751**	0.9653	0.9663	0.9731	0.9723	**0.9728**
Average	29.93	30.52	31.28	31.37	**31.46**	29.55	30.14	30.90	30.96	**31.12**	29.20	29.74	30.53	30.57	**30.62**
	0.9619	0.9598	0.9708	0.9713	**0.9723**	0.9593	0.9585	0.9688	0.9692	**0.9700**	0.9561	0.9541	0.9666	0.9669	**0.9679**

optimal performance, we set the same parameter values as set, heuristically, in the literature for the first and third steps of our proposed algorithm. We experimented by changing these parameter values but did not find any significant change in the results. The key parameter which connects independent components of the proposed algorithm is σ_p as discussed in Section. III-B. In the experiments, several parameters were set in the proposed AMNLRA method such as regularization parameter ζ, the parameter b, number of iteration L and patch size. The parameter ζ and b are set to 0.1 and $2\sqrt{2}$, respectively. The values of parameter m are set as 70, 90, 120 and 140 for $\sigma \leq 20$, $21 \leq \sigma \leq 40$, $41 \leq \sigma \leq 60$ and $\sigma > 60$, respectively. The size of search window is set 30×30. The number of iteration and the patch size are set according to the level of noise because for higher levels we need more number of patches as well as more number of iterations [6]. For the noise levels $\sigma \leq 20$, $20 < \sigma \leq 40$, $40 < \sigma \leq 60$ and $\sigma \geq 60$, we set the patch size to 6×6, 7×7, 8×8 and 9×9, respectively. For these noise level the number of iteration is set to 8, 12, 14 and 14, respectively.

TABLE 4. PSNR and FSIM comparison of the proposed algorithm (AMNLRA) with other methods for mixed noise (AWGN+RVIN), at $\sigma = 50$.

Image	$r = 20\%$			$r = 25\%$			$r = 30\%$			$r = 40\%$			$r = 50\%$		
	Cai et al.	WESNR	AMNLRA	Cai et al.	WESNR	AMNLRA	Cai et al.	WESNR	AMNLRA	Cai et al.	WESNR	AMNLRA	Cai et al.	WESNR	AMNLRA
Lena	22.98	24.73	**25.59**	22.55	24.32	**25.06**	22.04	23.79	**24.46**	20.87	22.44	**23.03**	19.61	21.10	**21.66**
	0.7810	0.8368	**0.8749**	0.7720	0.8310	**0.8693**	0.7579	0.8190	**0.8604**	0.7293	0.7902	**0.8390**	0.6969	0.7533	**0.8120**
Couple	22.12	22.93	**23.26**	21.73	22.62	**22.91**	21.34	22.27	**22.54**	20.40	21.41	**21.65**	19.30	20.31	**20.56**
	0.8099	0.8115	**0.8147**	0.7988	0.8051	**0.8076**	0.7903	0.8014	**0.8038**	0.7648	0.7744	**0.7594**	0.7339	0.7452	**0.7470**
Hill	22.58	23.87	**24.35**	22.12	23.47	**23.89**	21.60	23.00	**23.40**	20.41	21.78	**22.14**	19.08	20.45	**20.81**
	0.7837	0.8170	**0.8179**	0.7756	0.8060	**0.8080**	0.7638	0.7956	**0.8011**	0.7373	0.7727	**0.7838**	0.7089	0.7426	**0.7709**
Man	22.44	23.61	**24.01**	22.00	23.24	**23.63**	21.55	22.79	**23.17**	20.43	21.64	**21.95**	19.18	20.41	**20.73**
	0.7926	81.92	**83.31**	0.7819	81.36	**81.65**	0.7742	80.29	**80.81**	0.7474	77.84	**78.86**	0.7175	74.90	**76.80**
Boat	22.20	23.10	**23.48**	21.80	22.77	**23.11**	21.36	22.35	**22.67**	20.38	21.41	**21.66**	19.22	20.33	**20.60**
	0.7934	0.8118	**0.8258**	0.7839	0.8050	**0.8179**	0.7733	0.7936	**0.7963**	0.7477	0.7697	**0.7760**	0.7142	0.7385	**0.7513**
Fingerprint	19.86	20.35	**20.64**	19.49	19.94	**20.18**	19.10	19.48	**19.56**	18.25	18.56	**18.69**	17.31	17.61	**17.70**
	0.8414	0.8430	**0.8487**	0.8291	0.8312	**0.8331**	0.8309	0.8344	**0.8377**	0.7812	0.7979	**0.8011**	0.7614	0.7617	**0.7690**
Average	22.03	23.09	**23.55**	21.61	22.72	**23.13**	21.16	22.28	**22.63**	20.13	21.20	**21.52**	18.95	20.03	**20.32**
	0.8003	0.8232	**0.8358**	0.7902	0.8153	**0.8254**	0.7817	0.8078	**0.8179**	0.7512	0.7805	**0.7913**	0.7221	0.7483	**0.7697**

Algorithm 1 The Proposed Algorithm (AMNLRA) for Mixed Noise Removal

Input: Noisy image: u, Number of iterations: L
Mixed noise parameters: AWGN with σ; IN with $S\%$.

Initialize parameters as provided in Section. IV.
STEP-I.
Obtain median filtered image y using Eq. (10).
Identify IN pixels using Δ and R defined in Eqs. (11-12).
Obtain NLM filtered image u_n using Eq. (13).
Obtain preprocessed image u_p using Eq. (16).
STEP-II.
Estimate noise level σ_n in u_n using Eq. (18).
Use σ_n to estimate noise level σ_p defined in Eq. (19).
STEP-III.
Set k=1, Set $u_p^{(k)} = u_p$.
while $k \leq L$ **do**
  $u_p^{(k+1)} = u_p^{(k)} + \zeta\left(u_p - u_p^{(k)}\right)$.
  Construct patch matrix $\mathbf{U}_{p_i}$ using Eq. (21).
  Compute $[\mathbf{X}, \mathbf{D}, \mathbf{Y}] = svd\left(\mathbf{U}_{p_i}\right)$ using Eq. (23).
  Compute threshold weights w_i using Eq. (26).
  Apply thresholding operator T_{w_i} to $\mathbf{D}$ using Eq. (24).
  Obtain denoised patch matrix estimate $\hat{\mathbf{V}}_i$ using Eq. (27).
  Aggregate $\hat{\mathbf{V}}_i$ to obtain image $u_p^{(k+1)}$.
  k=k+1.
end while

Output: Denoised image: $v = u_p^{(L)}$

B. QUALITY MEASURES

In order to demonstrate the quantitative performance of AMNLRA, we evaluate features similarity index measure (FSIM) [55] and peak signal to noise ratio (PSNR) [56] values for the benchmark test images as shown in Fig. (2). PSNR values can be calculated using:

$$PSNR = 10log\frac{255^2}{MSE}, \tag{28}$$

where MSE is the mean square error and 255 is the maximum gray level of a 8 bits/pixel monochromatic image. Similarly, FSIM values can be calculated using:

$$FSIM = \frac{\sum_{x\in\Phi} S_L(x).PC_m(x)}{\sum_{x\in\Phi} PC_m(x)}, \tag{29}$$

where Φ is the spatial domain of the whole image, $S_L(x) = [S_{pc}(x)]^{\alpha}.[S_G(x)]^{\beta}$ is the overall similarity between the two compared images and $PC_m(x)$ is

$$PC_m(x) = max\{PC_1x, PC_2(x)\}, \tag{30}$$

where PC_1 and PC_2 are the maps extracted from the respective compared images.

C. QUANTITATIVE COMPARISON

The test images are corrupted by two kinds of mixed noise, namely AWGN+SPIN (AS) and AWGN+RVIN (AR). The quantitative performance are expressed in terms of PSNR and FSIM. Our experiments for each of (AS) and (AR) models include results for small and large values of AWGN and IN. The corresponding results for these small and large values are reported in separate tables for comprehensive analysis.

Table. 1 depicts PSNR and FSIM values for (AS) noise where the standard deviation of AWGN varies as $\sigma = 10$, 20 and 25 and SPIN ratio varies from $S = 30\%$ to 50% with step size of 10%. In this case, it can be observed that the proposed algorithm yields equivalent results for smaller values of either of the noise parameters σ and S. The equivalent performance may be justified in the sense that smaller S ratios may slight affect AWGN noise in the initial given image. Therefore, the preprocessed image, u_p, obtained in the first step of our proposed algorithm may not have significant contribution. However, as σ and/or S values increase beyond these smaller values, as shown in Table. 2, the proposed algorithm convincingly produces much better results than the compared methods in terms of both quality measures. In this case, AWGN distribution may be much affected by higher S ratio. Therefore, the first step of getting a preprocessed image, u_p, may have non-trivial contribution in producing significantly better results.

In case of (AR) noise comparison for lower values, Table 3 shows PSNR and FSIM results with $\sigma = 10$ whereas RVIN

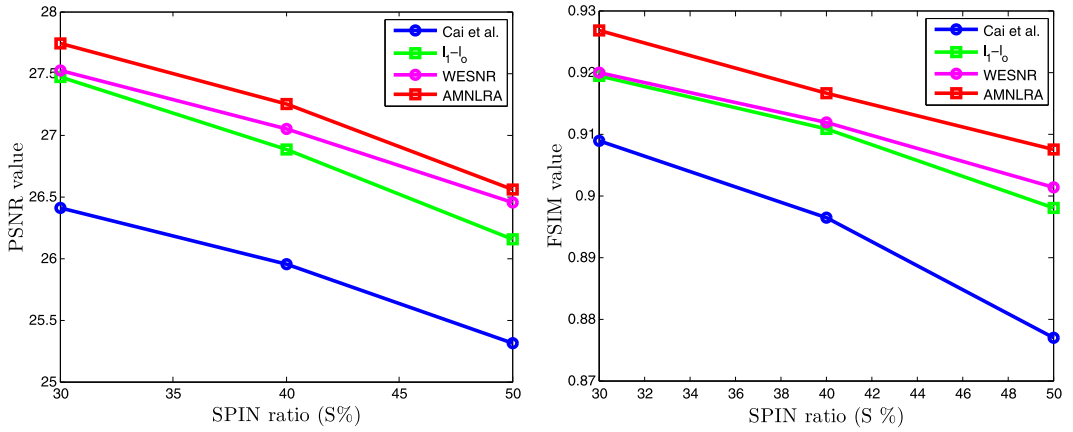

FIGURE 3. Graphical representation of average PSNR and FSIM values tabulated in Table 1. The graphs from left to right indicate average PSNR and average FSIM values, respectively, for (AWGN) parameter, $\sigma = 25$.

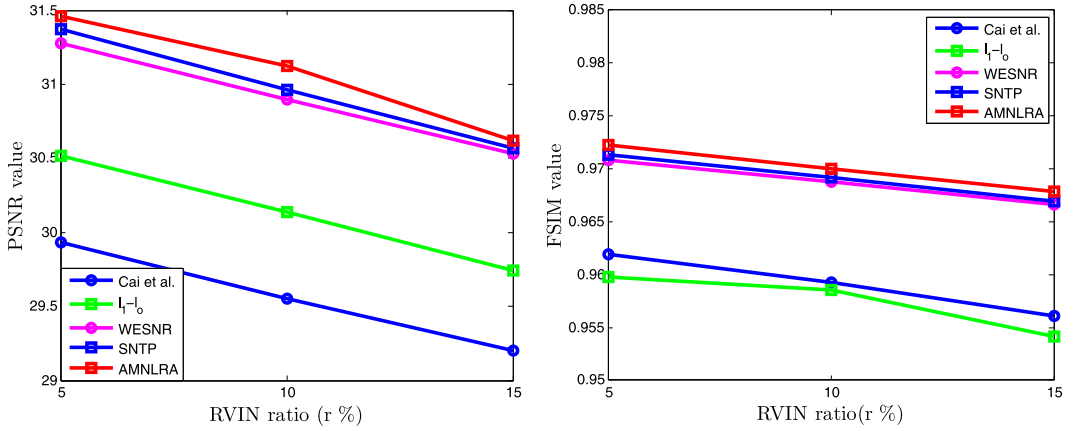

FIGURE 4. Graphical representation of average PSNR and FSIM values tabulated in Table 3. The graphs from left to right indicate average PSNR and average FSIM values, respectively, for (AWGN) parameter, $\sigma = 10$.

ratio varies from $r = 5\%$ to $r = 15\%$ with an incremental step of 5%. The proposed method achieves substantially better values of PSNR and FSIM than rest of the compared algorithms.

Lastly, the comparison of the proposed algorithm for higher σ and $r\%$ values are reported in Table. 4. Here, we set noise parameter $\sigma = 50$ and allow RVIN ratio $r\%$ to vary from 20% to 50%. Again, the proposed algorithm significantly outperforms the compared algorithms. For more precise visualisation of the tabulated comparison, average PSNR and FSIM values at $\sigma = 25$ are shown for (AS) and (AR) noise models in Fig. 3 and Fig. 4, respectively.

D. QUALITATIVE COMPARISON

In addition to quantitative comparison, we conducted the visual comparison of AMNLRA with Cai *et al.* [22] and WESNR [17] for sake of qualitative analysis. In this respect, Fig.5 represents the denoising results of the Cameraman test image effected by AWGN+SPIN($\sigma = 25$, $S = 40\%$) noise model. The visual result clearly reflect the superior performance of the proposed algorithm than compared state-of-the-art algorithms. It can be observed in the magnified sub-images that Cai *et al.* [22] caused some extra structures and diffused the edges of the camera with the sky background as well. Similarly, WESNR has converted the light gray region near the lens of camera into completely black region. However, the proposed algorithm preserve the edges in a much better way. In Fig.6, we used the high values of $\sigma = 50$ and SPIN ratio $S = 50\%$. In this case, the performance of WESNR has worsened as it produced lots of artifacts. Cai *et al.* [22] comparatively performs better than WESNR, yet the image structure has been significantly diffused as shown in the magnified sub-image. On the other hand, the proposed method performs much better in recovering the image structure without producing any significant artifact.

In Figs. 7 and 8, visual comparisons are presented for house and Barbara test images, respectively, which are affected by AWGN+RVIN noise. The noise parameters are, respectively, set as $\sigma = 20$ and 50 for AWGN, while $r = 30\%$ and 50% for RVIN. The denoising results are similar to those for AWGN+SPIN noise, discussed earlier. Particularly, in case of Barbara image shown in Fig. 8, the texture pattern of table

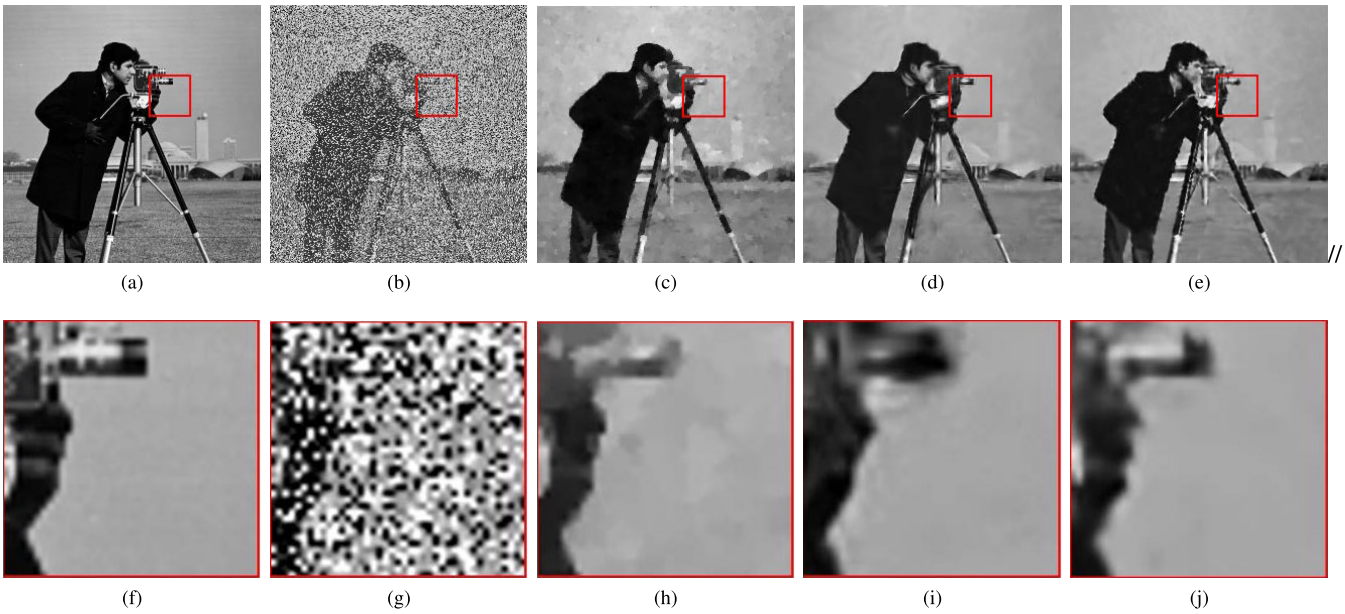

FIGURE 5. Denoising results. (a) Original noise free image, (b) Image corrupted by mixed noise AWGN+SPIN($\sigma = 25$, $S = 40\%$), (c) Cai *et al.* [22], (d) WESNR [17], (e) AMNLRA algorithm. Bottom row from left to right shows magnified version of the selected red colored region of the of the above images.

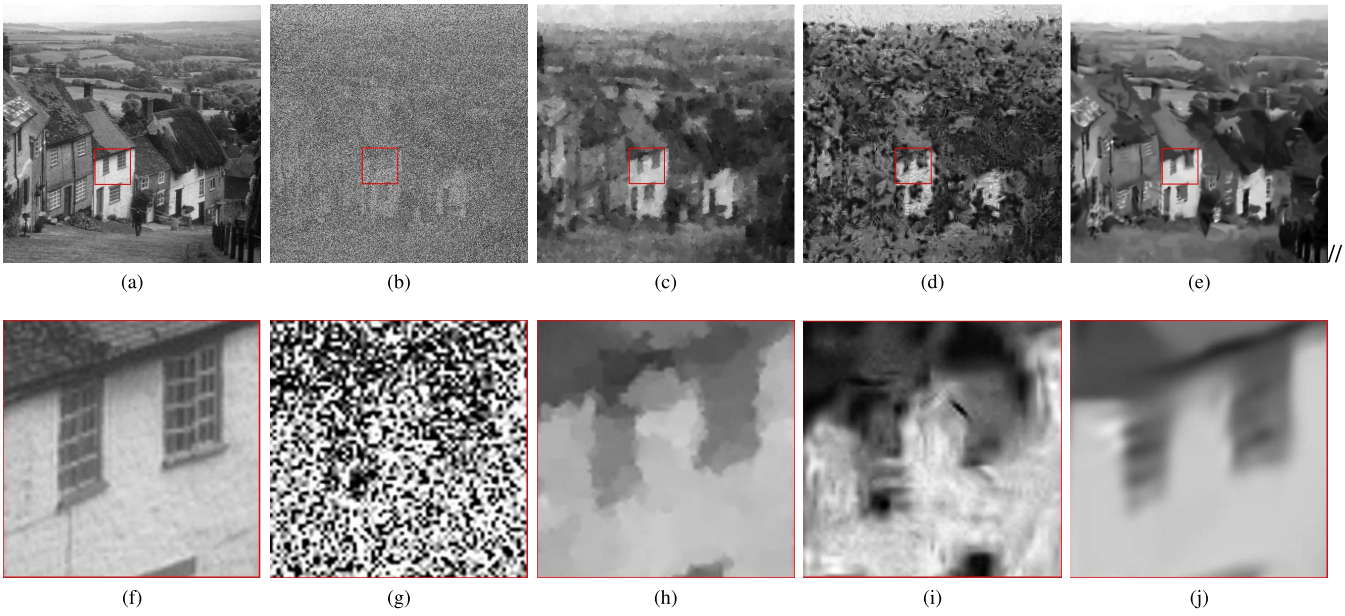

FIGURE 6. Denoising results. (a) Original noise free image, (b) Image corrupted by mixed noise AWGN+SPIN($\sigma = 50$, $S = 50\%$), (c) Cai *et al.* [22], (d) WESNR [17], (e) AMNLRA algorithm. Bottom row from left to right shows magnified version of the selected red colored region of the of the above images.

cover has been completely buried in noise. Cai *et al.* [22] and WESNR can only recover a fraction of that textured region along with lots of artifacts whereas the proposed algorithm, somehow, succeeded in preserving more details. Furthermore, the proposed algorithm performs well in order to retain edge structure. It can be observed from the house image shown in Fig. 7 (c)-(d) that edge structure has been diffused and smeared by Cai *et al.* [22] and WESNR while producing lots of artifacts at the same time region between the edges. Whereas, the proposed algorithm has retained the details of edge structure without inducing artifacts. In addition, Fig. 9 and Fig. 10 show the denoising comparison for camera and house test image by varying AWGN parameter σ, SPIN parameter $s\%$ and RVIN parameter $r\%$, respectively. It can therefore be noticed from the visual comparison that the above qualitative comparison is compatible with our quantitative analysis as well, confirming the better performance of the proposed algorithm.

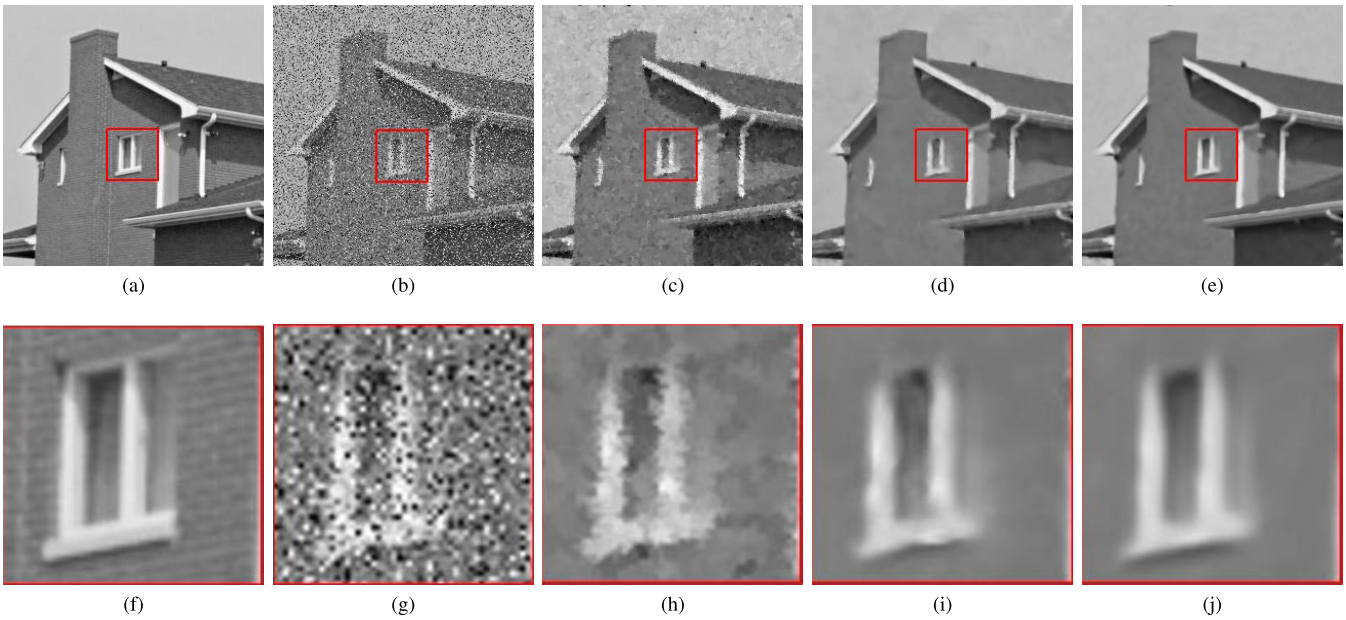

FIGURE 7. Denoising results. (a) Original noise free image, (b) Image corrupted by mixed noise AWGN+RVIN($\sigma = 20$, $r = 30\%$), (c) Cai *et al.* [22], (d) WESNR [17], (e) AMNLRA algorithm. Bottom row from left to right shows magnified version of the selected red colored region of the of the above images.

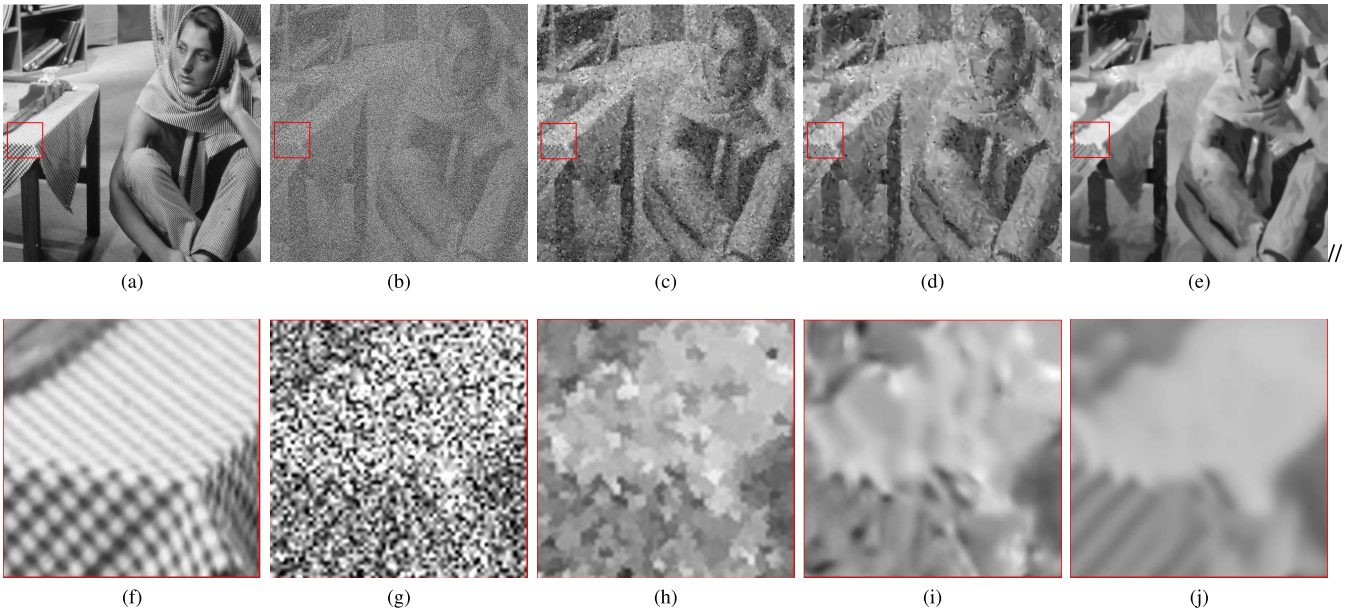

FIGURE 8. Denoising results. (a) Original noise free image, (b) Image corrupted by mixed noise AWGN+RVIN ($\sigma = 50$, $r = 50\%$), (c) Cai *et al.* [22], (d) WESNR [17], (e) AMNLRA algorithm. Bottom row from left to right shows magnified version of the selected red colored region of the of the above images.

E. TIME COMPLEXITY

Time complexity of the proposed algorithm has three major factors corresponding to computation of adaptive median filtering (AMF), non-local means filtering (NLM) and low rank approximation (LRA), respectively. The basic operation during AMF is to order the pixels within the neighborhood of referenced pixel location. In case of image with size $n \times n$, the sorting complexity is $O(n \log_2 n)$ [57]. In case of NLM step, time complexity is $O(n^2wp)$ where w and p denote the size of search window and patch size, respectively [44]. Lastly, the time complexity of LRA step consists of two major sources namely, patch comparison (block matching) and singular value thresholding. The corresponding time complexities of these dominant components are $O(pqrs)$ and $O(psr \min(p, s))$, respectively, where r represents number of reference patches selected for LRA, s represents number of similar patches for a given reference patch and q is the number of patches within the search window [33]. Thus the time

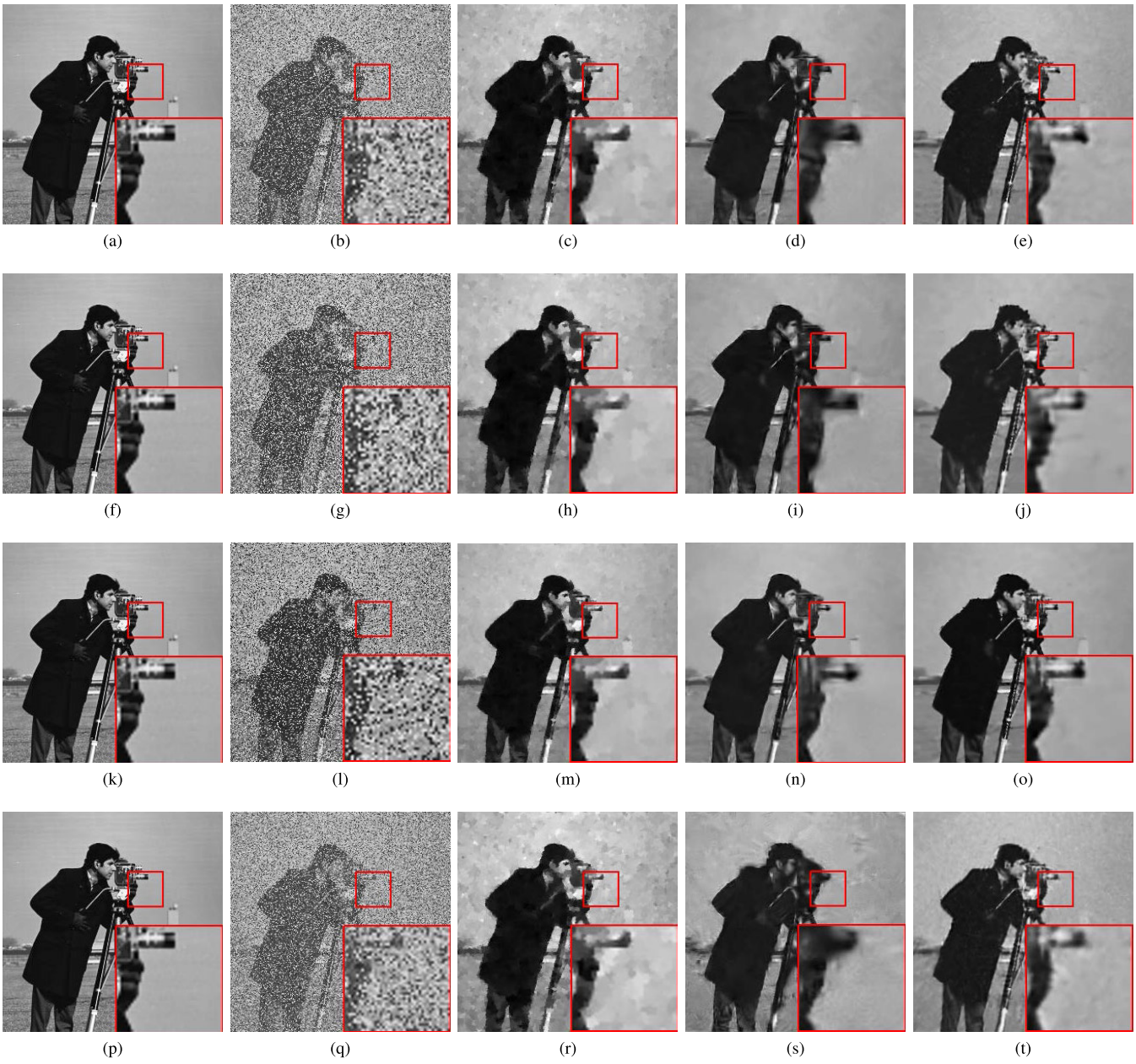

FIGURE 9. Images from left to right represent the original noise free image, image corrupted by mixed noise AWGN+RVIN, denoising results of Cai *et al.* [22], WESNR [17] and AMNLRA algorithm respectively. Images from top to bottom represent the denoising results for mixed noise ($\sigma = 30, S = 30\%$), ($\sigma = 30, S = 40\%$), ($\sigma = 20, r = 30\%$) and ($\sigma = 40, S = 30\%$), respectively.

TABLE 5. Running time comparison (in seconds) for mixed noise (AWGN+SPIN), at $S = 30\%$.

	$\sigma = 10$			$\sigma = 30$			$\sigma = 50$		
Image	Cai et al.	WESNR	AMNLRA	Cai et al.	WESNR	AMNLRA	Cai et al.	WESNR	AMNLRA
Lena	122	103	646	179	167	773	245	166	987
Barbara	162	75	483	186	123	765	256	124	961
House	28	30	115	42	45	137	49	48	196
Man	133	104	501	191	190	771	252	130	981
Average	111	78	436	149	131	612	200	117	781

complexity of the proposed algorithm is sum of the above mentioned individual time complexities. It can be noticed that time complexities of AMF and NLM steps are negligible as compared to that of LRA step due to block matching and singular value thresholding mechanism. The computational time comparison of the proposed algorithm is depicted in Table. 5. It can be observed that on average WESNR has the lowest time complexity. It is due to the fact that WESNR

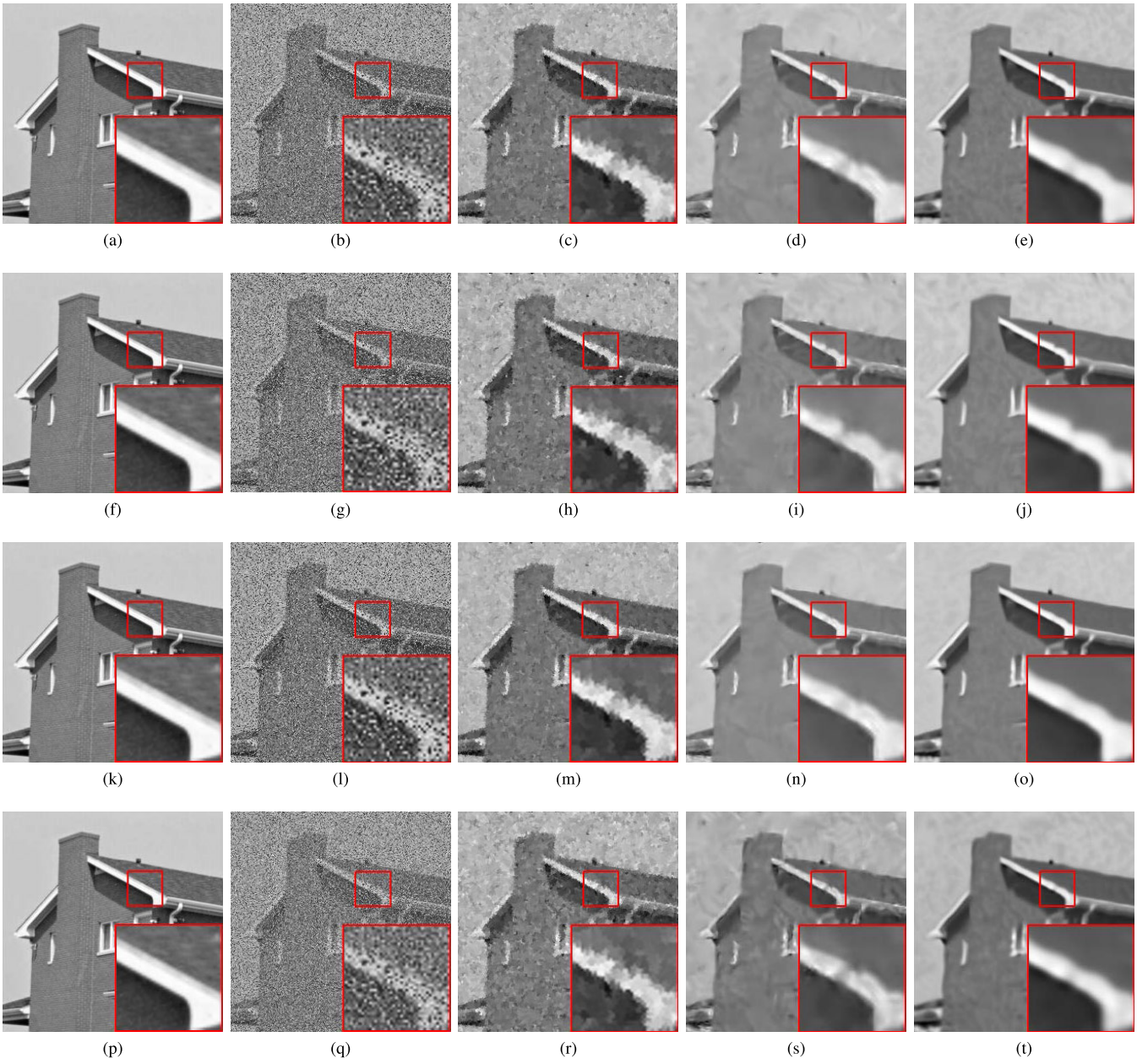

FIGURE 10. Image from left to right represent the original noise free image, image corrupted by mixed noise AWGN+RVIN, denoising results of Cai *et al.* [22], WESNR [17] and AMNLRA algorithm respectively. Images from top to bottom represent the denoising results for mixed noise ($\sigma = 30, r = 30\%$), ($\sigma = 30, r = 40\%$), ($\sigma = 25, r = 30\%$) and ($\sigma = 40, r = 30\%$), respectively.

employs off-line dictionary learning technique. The computational cost of the proposed algorithm is significantly higher than rest of the algorithms. As explained earlier, the increased time complexity originates from computationally intensive block matching and singular value thresholding processes. However, the cost can be reduced by parallel implementation of blockmatching as carried out in [3].

V. CONCLUSION

In this paper, we provided a novel mechanism for the removal of mixed noise which consists of three important steps. We tried to explain how a complex problem of mixed noise removal, with different noise statistics, can be first transformed in to a simpler problem of mixed noise statistics of same type (Gaussian noise). This step has enabled the proposed algorithm achieve much better results in the presence of severe noise levels. However, it turned out that above mentioned transformation step has less significance in case of smaller values of impulse noise. We justified these outcomes with the argument that smaller values of impulse noise did not have significant effect on Gaussianity of AWGN noise in the given image. Therefore, the results with or without preprocessed image are almost equivalent. Furthermore, it is worth noticing that getting a preprocessed image is not

sufficient for subsequent denoising process until and unless noise variance is not estimated. To this end, we utilized an effective patch based noise estimation approach which constitutes a special type of covariance matrix depending upon weak texture patches. The smallest eigenvalue of this covariance matrix reflected the estimated noise variance. Once the involved problem had been reduced to a relatively simpler one, we were able to employ well known image priors like non-local self similarity and low rank approximation to finally recover the underlying true image. Experimental results, in terms of quantitative and qualitative comparisons, have provided convincing evidence of better denoising capability of the propose algorithm as compared to various outstanding algorithms.

AKNOWLEDGMENT

ZHS would like to thank Department of Mathematics, University of the Punjab, Lahore for the partial support. AM would like to acknowledge the support of Mathematics Teaching and Learning, research group within the Department of Mathematics, FLU, Nord University, Bodø.

REFERENCES

[1] C. Tomasi and R. Manduchi, "Bilateral filtering for gray and color images," in *Proc. 6th Int. Conf. Comput. Vis.*, 1998, pp. 839–846.

[2] A. Buades, B. Coll, and J.-M. Morel, "A non-local algorithm for image denoising," in *Proc. IEEE Comput. Soc. Conf. Comput. Vis. Pattern Recognit. (CVPR)*, vol. 2, Jun. 2005, pp. 60–65.

[3] K. Dabov, A. Foi, V. Katkovnik, and K. Egiazarian, "Image denoising by sparse 3-D transform-domain collaborative filtering," *IEEE Trans. Image Process.*, vol. 16, no. 8, pp. 2080–2095, Aug. 2007.

[4] W. Dong, G. Shi, and X. Li, "Nonlocal image restoration with bilateral variance estimation: A low-rank approach," *IEEE Trans. Image Process.*, vol. 22, no. 2, pp. 700–711, Feb. 2013.

[5] W. Dong, L. Zhang, and G. Shi, "Centralized sparse representation for image restoration," in *Proc. Int. Conf. Comput. Vis.*, Nov. 2011, pp. 1259–1266.

[6] S. Gu, L. Zhang, W. Zuo, and X. Feng, "Weighted nuclear norm minimization with application to image denoising," in *Proc. IEEE Conf. Comput. Vis. Pattern Recognit.*, Jun. 2014, pp. 2862–2869.

[7] R. H. Chan, Chung-Wa, and M. Nikolova, "Salt-and-pepper noise removal by median-type noise detectors and detail-preserving regularization," *IEEE Trans. Image Process.*, vol. 14, no. 10, pp. 1479–1485, Oct. 2005.

[8] P.-E. Ng and K.-K. Ma, "A switching median filter with boundary discriminative noise detection for extremely corrupted images," *IEEE Trans. Image Process.*, vol. 15, no. 6, pp. 1506–1516, Jun. 2006.

[9] H.-M. Lin and A. N. Willson, "Median filters with adaptive length," *IEEE Trans. Circuits Syst.*, vol. 35, no. 6, pp. 675–690, Jun. 1988.

[10] S.-J. Ko and Y. H. Lee, "Center weighted median filters and their applications to image enhancement," *IEEE Trans. Circuits Syst.*, vol. 38, no. 9, pp. 984–993, Sep. 1991.

[11] H. Ji, C. Liu, Z. Shen, and Y. Xu, "Robust video denoising using low rank matrix completion," in *Proc. IEEE Comput. Soc. Conf. Comput. Vis. Pattern Recognit.*, Jun. 2010, pp. 1791–1798.

[12] E. López-Rubio, "Restoration of images corrupted by Gaussian and uniform impulsive noise," *Pattern Recognit.*, vol. 43, no. 5, pp. 1835–1846, May 2010.

[13] R. W. Liu, L. Shi, S. C. H. Yu, and D. Wang, "Box-constrained second-order total generalized variation minimization with a combined L_1, 2 data-fidelity term for image reconstruction," *J. Electron. Imag.*, vol. 24, no. 3, Jun. 2015, Art. no. 033026.

[14] C. Zhang, D. Wu, R. W. Liu, and N. Xiong, "Non-local regularized variational model for image deblurring under mixed Gaussian-impulse noise," *Internet Technol. J.*, vol. 16, no. 7, pp. 1301–1319, 2015.

[15] R. W. Liu, L. Shi, W. Huang, J. Xu, S. C. H. Yu, and D. Wang, "Generalized total variation-based MRI rician denoising model with spatially adaptive regularization parameters," *Magn. Reson. Imag.*, vol. 32, no. 6, pp. 702–720, Jul. 2014.

[16] L. Liu, H. Yang, J. Fan, R. W. Liu, and Y. Duan, "Rician noise and intensity nonuniformity correction (NNC) model for MRI data," *Biomed. Signal Process. Control*, vol. 49, pp. 506–519, Mar. 2019.

[17] J. Jiang, L. Zhang, and J. Yang, "Mixed noise removal by weighted encoding with sparse nonlocal regularization," *IEEE Trans. Image Process.*, vol. 23, no. 6, pp. 2651–2662, Jun. 2014.

[18] R. Garnett, T. Huegerich, C. Chui, and W. He, "A universal noise removal algorithm with an impulse detector," *IEEE Trans. Image Process.*, vol. 14, no. 11, pp. 1747–1754, Nov. 2005.

[19] I. Markovsky and K. Usevich, *Low Rank Approximation*, vol. 139. Cham, Switzerland: Springer, 2012.

[20] G. Liu, Z. Lin, S. Yan, J. Sun, Y. Yu, and Y. Ma, "Robust recovery of subspace structures by low-rank representation," *IEEE Trans. Pattern Anal. Mach. Intell.*, vol. 35, no. 1, pp. 171–184, Jan. 2013.

[21] H. Hwang and R. A. Haddad, "Adaptive median filters: New algorithms and results," *IEEE Trans. Image Process.*, vol. 4, no. 4, pp. 499–502, Apr. 1995.

[22] J.-F. Cai, R. H. Chan, and M. Nikolova, "Two-phase approach for deblurring images corrupted by impulse plus Gaussian noise," *Inverse Problems Imag.*, vol. 2, no. 2, p. 187, 2008.

[23] Y. Xiao, T. Zeng, J. Yu, and M. K. Ng, "Restoration of images corrupted by mixed Gaussian-impulse noise via l1–l0 minimization," *Pattern Recognit.*, vol. 44, no. 8, pp. 1708–1720, Aug. 2011.

[24] J. Liu, X.-C. Tai, H. Huang, and Z. Huan, "A weighted dictionary learning model for denoising images corrupted by mixed noise," *IEEE Trans. Image Process.*, vol. 22, no. 3, pp. 1108–1120, Mar. 2013.

[25] J. Jiang, J. Yang, Y. Cui, and L. Luo, "Mixed noise removal by weighted low rank model," *Neurocomputing*, vol. 151, pp. 817–826, Mar. 2015.

[26] J. Tukey, "Nonlinear (nonsuperposable) methods for smoothing data," in *Proc. Cong. Rec. EASCOM*, 1974, pp. 673–681.

[27] G. Gupta, "Algorithm for image processing using improved median filter and comparison of mean, median and improved median filter," *Int. J. Soft Comput. Eng.*, vol. 1, no. 5, pp. 304–311, 2011.

[28] J.-H. Wang and L.-D. Lin, "Improved median filter using minmax algorithm for image processing," *Electron. Lett.*, vol. 33, no. 16, pp. 1362–1363, Jul. 1997.

[29] P. K. Sinha and Q. H. Hong, "An improved median filter," *IEEE Trans. Med. Imag.*, vol. 9, no. 3, pp. 345–346, Sep. 1990.

[30] Y. Zhu and C. Huang, "An improved median filtering algorithm for image noise reduction," *Phys. Procedia*, vol. 25, pp. 609–616, 2012.

[31] Y. Chen and M. J. Wainwright, "Fast low-rank estimation by projected gradient descent: General statistical and algorithmic guarantees," 2015, *arXiv:1509.03025*. [Online]. Available: http://arxiv.org/abs/1509.03025

[32] Z. Liu, L. Yu, and H. Sun, "Image denoising via nonlocal low rank approximation with local structure preserving," *IEEE Access*, vol. 7, pp. 7117–7132, 2019.

[33] H. Yang, Y. Park, J. Yoon, and B. Jeong, "An improved weighted nuclear norm minimization method for image denoising," *IEEE Access*, vol. 7, pp. 97919–97927, 2019.

[34] D.-G. Kim and Z. H. Shamsi, "Enhanced residual noise estimation of low rank approximation for image denoising," *Neurocomputing*, vol. 293, pp. 1–11, Jun. 2018.

[35] S. Liu, Q. Hu, P. Li, J. Zhao, M. Liu, and Z. Zhu, "Speckle suppression based on weighted nuclear norm minimization and grey theory," *IEEE Trans. Geosci. Remote Sens.*, vol. 57, no. 5, pp. 2700–2708, May 2019.

[36] S. Liu, M. Liu, P. Li, J. Zhao, Z. Zhu, and X. Wang, "SAR image denoising via sparse representation in shearlet domain based on continuous cycle spinning," *IEEE Trans. Geosci. Remote Sens.*, vol. 55, no. 5, pp. 2985–2992, May 2017.

[37] C. Wang, Z. Zhu, H. Gu, X. Wu, and S. Liu, "Hankel low-rank approximation for seismic noise attenuation," *IEEE Trans. Geosci. Remote Sens.*, vol. 57, no. 1, pp. 561–573, Jan. 2019.

[38] E. J. Candès, X. Li, Y. Ma, and J. Wright, "Robust principal component analysis?" *J. ACM*, vol. 58, no. 3, pp. 11:1–11:37, May 2011.

[39] H. Ji, S. Huang, Z. Shen, and Y. Xu, "Robust video restoration by joint sparse and low rank matrix approximation," *SIAM J. Imag. Sci.*, vol. 4, no. 4, pp. 1122–1142, Jan. 2011.

[40] Z. Liu, J. Wang, G. Liu, and J. Pu, "Sparse low-rank preserving projection for dimensionality reduction," *IEEE Access*, vol. 7, pp. 22941–22951, 2019.

[41] L. Xinyan, M. Jie, Z. Xiaomei, and H. Zhaozheng, "Image denoising of low-rank matrix recovery via joint frobenius norm," *J. Image Graph.*, vol. 19, no. 4, pp. 502–511, 2014.
[42] L. T. Nguyen, J. Kim, and B. Shim, "Low-rank matrix completion: A contemporary survey," *IEEE Access*, vol. 7, pp. 94215–94237, 2019.
[43] Z. Yuan, X. Lin, and X. Wang, "The LSE model to denoise mixed noise in images," *J Signal Process*, vol. 29, no. 10, pp. 1329–1335, 2013.
[44] Z. H. Shamsi and D.-G. Kim, "Multiscale hybrid nonlocal means filtering using modified similarity measure," *Math. Problems Eng.*, vol. 2015, pp. 1–17, Nov.2015.
[45] D. L. Donoho, "De-noising by soft-thresholding," *IEEE Trans. Inf. Theory*, vol. 41, no. 3, pp. 613–627, May 1995.
[46] D. L. Donoho and I. M. Johnstone, "Adapting to unknown smoothness via wavelet shrinkage," *J. Amer. Stat. Assoc.*, vol. 90, no. 432, pp. 1200–1224, Dec. 1995.
[47] M. Hashemi and S. Beheshti, "Adaptive noise variance estimation in BayesShrink," *IEEE Signal Process. Lett.*, vol. 17, no. 1, pp. 12–15, Jan. 2010.
[48] S. I. Olsen, "Estimation of noise in images: An evaluation," *CVGIP, Graph. Models Image Process.*, vol. 55, no. 4, pp. 319–323, Jul. 1993.
[49] G. Chen, F. Zhu, and P. A. Heng, "An efficient statistical method for image noise level estimation," in *Proc. IEEE Int. Conf. Comput. Vis. (ICCV)*, Dec. 2015, pp. 477–485.
[50] M. M. Ghazi and H. Erdogan, "Image noise level estimation based on higher-order statistics," *Multimedia Tools Appl.*, vol. 76, no. 2, pp. 2379–2397, Jan. 2017.
[51] P. Jiang and J.-Z. Zhang, "Fast and reliable noise level estimation based on local statistic," *Pattern Recognit. Lett.*, vol. 78, pp. 8–13, Jul. 2016.
[52] A. Khmag, S. A. R. Al-haddad, and N. Kamarudin, "Natural image noise level estimation based on local statistics for blind noise reduction," *Vis. Comput.*, vol. 34, no. 4, pp. 575–587, 2018.
[53] X. Liu, M. Tanaka, and M. Okutomi, "Noise level estimation using weak textured patches of a single noisy image," in *Proc. 19th IEEE Int. Conf. Image Process.*, Sep. 2012, pp. 665–668.
[54] J. Jiang, J. Yang, Y. Cui, W. K. Wong, and Z. Lai, "Sparse nonlocal priors based two-phase approach for mixed noise removal," *Signal Process.*, vol. 116, pp. 101–111, Nov. 2015.
[55] L. Zhang, L. Zhang, X. Mou, and D. Zhang, "FSIM: A feature similarity index for image quality assessment," *IEEE Trans. Image Process.*, vol. 20, no. 8, pp. 2378–2386, Aug. 2011.
[56] A. Hore and D. Ziou, "Image quality metrics: PSNR vs. SSIM," in *Proc. 20th Int. Conf. Pattern Recognit.*, Aug. 2010, pp. 2366–2369.
[57] B.-G. Huang, Z.-T. Lu, C.-M. Ma, and J.-X. Zhao, "Improved adaptive median filtering algorithm," *J. Comput. Appl.*, vol. 31, no. 7, pp. 1836–1837, 2011.

DAI-GYOUNG KIM received the Ph.D. degree in applied mathematics from Purdue University, in 1994. He did his Postdoctoral Research with IMA, University of Minnesota, in 1995. He was a Visiting Scholar with the Image Processing Group, UCLA, from 2003 to 2004. He is currently a Professor with the Department of Applied Mathematics and a joint Professor with the Department of Artificial Intelligence, Hanyang University, South Korea. His research interests include numerical PDE, optimizations, data processing, deep learning, and quantum computations, as well as scientific computations in Industry.

MUKHTAR HUSSAIN received the B.S. degree (Hons.) in applied mathematics from Government College University, Faisalabad, Pakistan, in 2018. He is currently pursuing the M.Phil. degree in computational mathematics from the University of the Punjab, Pakistan, under the supervision of Dr. Z. H. Shamsi. His research interests include computer vision, image processing, machine learning, and numerical analysis.

MUHAMMAD ADNAN received the B.S. degree in mathematics from the University of the Punjab, Pakistan, in 2018, where he is currently pursuing the M.Phil. degree in computational mathematics, under the supervision of Dr. Z. H. Shamsi. His research interests include image processing, machine learning, and numerical analysis.

MUHAMMAD ASIF FAROOQ received the Ph.D. degree from NTNU, Norway, in 2012. He has been working as an Assistant Professor with the School of Natural Sciences, National University of Sciences and Technology, Islamabad, Pakistan, since 2012. His research interests include computational fluid dynamics and numerical analysis.

ZAHID HUSSAIN SHAMSI received the M.Sc. degree in mathematics and the M.Sc. degree in computer science from the University of the Punjab, Pakistan, in 2000 and 2003, respectively, and the Ph.D. degree in applied mathematics from Hanyang University, South Korea, in 2016, for which he was awarded prestigious HEC scholarship by Government of Pakistan. He is currently an Assistant Professor with the Department of Mathematics, University of the Punjab. His research interests include image processing, machine learning, quantum information theory, relativistic quantum information, and quantum machine learning.

ASIF MUSHTAQ received the Ph.D. degree in mathematical sciences from NTNU, Trondheim, Norway, in 2014. He is currently working as an Associate Professor in mathematics with Nord University, Norway. He was a Postdoctoral Fellow with Sintef ICT and with the Department of Mathematical Sciences, NTNU. His areas of interest include applied mathematics, mathematics education, and computational mathematics.